Modeling of Thermal Transport in Pillared-Graphene Architectures

Vikas Varshney,[†,§,*] Soumya S. Patnaik,[‡] Ajit K. Roy,[†,*] George Froudakis,[⊥] and Barry L. Farmer[†]

[†]Materials and Manufacturing Directorate and, [‡]Propulsion Directorate, Air Force Research Laboratory, Wright Patterson Air Force Base, Dayton, Ohio, [§]Universal Technology Corporation, Dayton, Ohio, and [⊥]Department of Chemistry, University of Crete, Greece

ABSTRACT Carbon nanotubes (CNT) and graphene are considered as potential future candidates for many nano/microscale integrated devices due to their superior thermal properties. Both systems, however, exhibit significant anisotropy in their thermal conduction, limiting their performance as three-dimensional thermal transport materials. From thermal management perspective, one way to tailor this anisotropy is to consider designing alternative carbon-based architectures. This paper investigates the thermal transport in one such novel architecture—a pillared-graphene (PG) network nanostructure which combines graphene sheets and carbon nanotubes to create a three-dimensional network. Nonequilibrium molecular dynamics simulations have been carried out using the AIREBO potential to calculate the thermal conductivity of pillared-graphene structures along parallel (in-plane) as well as perpendicular (out-of-plane) directions with respect to the graphene plane. The resulting thermal conductivity values for PG systems are discussed and compared with simulated values for pure CNT and graphite. Our results show that in these PG structures, the thermal transport is governed by the minimum interpillar distance and the CNT—pillar length. This is primarily attributed to scattering of phonons occurring at the CNT—graphene junctions in these nanostructures. We foresee that such architecture could potentially be used as a template for designing future structurally stable microscale systems with tailorable in-plane and out-of-plane thermal transport.

KEYWORDS: pillared-graphene · carbon nanotubes · graphene · molecular dynamics · thermal transport · phonon scattering · thermal management.

In the past few years, the issue of thermal management has received significant attention from the electronics and the aerospace industry.[1,2] With the development of micro/nanoscale electronic devices,[3,4] the need to quickly dissipate thermal energy is absolutely critical for device performance and lifetime.[5] The aerospace industry too has issues managing waste heat, generated from various electronic and mechanical components within aircrafts. These concerns have provided motivation to understand, improve, and guide the development of novel materials with tailored multidimensional thermal transport characteristics, which are an integral part of current aerospace and electronics industry. Recently, directional thermal transport has also garnered a lot of interest in the area of thermal rectification phenomenon[6] and phonon waveguides[7] to address these issues.

It is well-known from many experimental evidences that carbon nanotubes (CNT), graphene, and diamond are a few of the excellent thermally conductive known materials. The superior thermal conductivity of these carbon allotropes[8−12] is attributed to their ordered structure as well as to the stiffness of C−C bonds. However, unlike diamond, which exhibits isotropic thermal conductivity due to its tetrahedral bonding network, other forms of allotropic carbon (CNT, graphite) have direction dependent thermal transport properties. The thermally conductive direction for CNT is along its cylindrical axis, whereas for graphite, dominant thermal conduction is along the graphene plane. In both the systems, the thermal conductivity in the corresponding perpendicular direction is reduced by two or more orders of magnitude.[13−15] This is due to the fact that in transverse direction the graphene sheets/nanotubes interact only *via* nonbonded van der Waals interactions. When these allotropes (CNT/graphite) are introduced as fillers/additives in polymer composites, only a minor enhancement is observed in the effective value of thermal conductivity. As these fillers are randomly dispersed in the matrix, they almost always come in transverse contact over a relatively less contact area, leading to very high thermal resistivity.[16] Even for randomly oriented pure CNT-pallets, theoretical calculations using Green's function have determined the upper-bound of overall thermal conductivity to be only a few W/m-K.[17] Therefore, to avoid/overcome these thermal barriers, it is important to design new interfacial architectures with inherently low thermal interface resistance.

*Address correspondence to vikas.varshney@afmcx.net, ajit.roy@wpafb.af.mil.

Received for review October 1, 2009 and accepted January 15, 2010.

Published online January 29, 2010. 10.1021/nn901341r

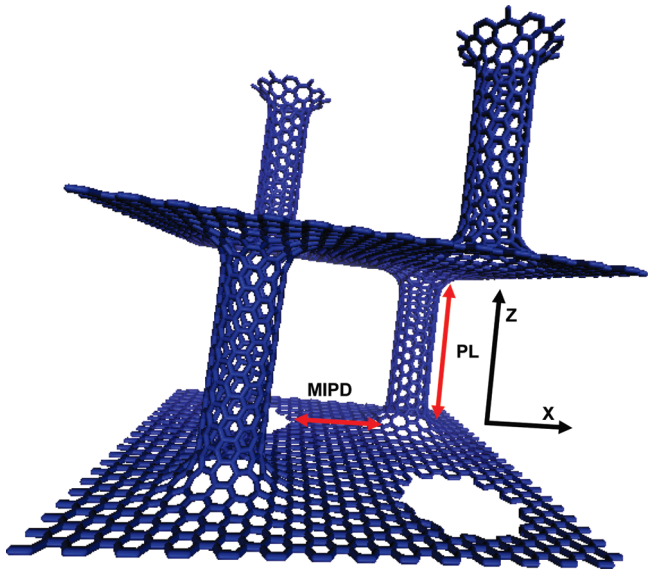

Figure 1. Schematic of a pillared-graphene system. MIPD and PL correspond to minimum interpillar distance and pillar length, respectively. Minimum interpillar distance was calculated as MIPD = (system dimension along *X*-direction)/2 − CNT diameter. Pillar length was assumed to be the distance between two graphene sheets.

For example, in principle, two graphene sheets could be bonded together by a linkage to increase out-of-plane thermal transport. Such design scheme can however give rise to few very simple, yet significant questions: (a) How does the inclusion of such *linkers or bonded network* affect the *out-of-plane* as well as *in-plane* thermal transport properties in graphene sheets? (b) Does the *dimension* of such a network play significant role toward determining its overall thermal transport properties? (c) What is the significance of the *length* of such a linker on the thermal transport?

To appreciate aforementioned concerns, one must first consider; "How should we link two graphene sheets to each other in a thermally effective manner?" In this regard, exfoliation with compatible polymer matrix followed by graphitic functionalization is one possible route to achieve such a linkage.[18,19] However, due to intrinsic low thermal conductivity of polymer matrix, the heat transport across the graphene sheets is still expected to be significantly low. To achieve better thermal transport in perpendicular direction, carbon nanotubes (due to their high thermal conductivity in axial direction) could emerge as an attractive candidate in the form of a CNT−graphene junction to create what is known as "pillared-graphene" architecture. Froudakis *et al*. have recently investigated this architecture from the perspective of hydrogen storage.[20] Not only did they postulate that such a structure is energetically stable based on quantum mechanical studies, they also predicted that such a morphology could be used very efficiently for hydrogen storage reaching Department of Energy (DOE) requirements. Recently, Li *et al*. have also investigated the electronic transport on similar CNT−graphene junctions using nonequilibrium Green's function approach.[21] While former junctions[20] were built entirely of sp^2 carbon atoms, latter[21] employed heterojunctions with short molecular linkers, linking CNT and graphene. Several other novel carbon-based architectures have also been investigated recently from the viewpoint of electronic transport[22] and thermal rectification.[23−26] The synthesis efforts in similar carbon nanotube intramolecular junctions have also been reviewed recently.[27]

From the perspective of thermal transport in such a novel architecture (pillared-graphene system), it is intuitive to imagine significant heat transport in graphene plane direction as well as nanotube axis direction at first. Since both nanotubes and graphene sheet are built from the same constitutive element "carbon" as well as have same hybridization, the nanotube−graphene junction—if built purely from carbon atoms as in ref 20—is expected to exhibit low thermal resistance. In this study, we have explored the potential of such architecture from the perspective of heat transport using atomistic molecular dynamics (MD) simulations. MD simulations have been used to simulate thermal transport of a wide variety of systems which include carbon nanotubes and graphene,[13,14,28−30] diamond,[31,32] ionic solids,[33] crystalline and amorphous silicon,[34,35] silica,[36] metals,[37] layered-structures,[38,39] nanocomposites,[40] network polymers,[41] and argon films[42] using the Green−Kubo approach[43] (equilibrium molecular dynamics) and Fourier law approach[44] (nonequilibrium molecular dynamics). In this article, we plan to investigate how the "CNT−pillared-graphene morphology" affects the out-of-plane thermal transport of graphene sheets, along with additional aforementioned concerns, using the nonequilibrium molecular dynamics (NEMD) simulations.

The simulations were performed on three sets of pillared-graphene structures (PGS) having different values of graphene interlayer distance (CNT−pillar length) and separation distance between the nanotube pillars (interpillar distance). The unit cell of one of these systems is shown schematically in Figure 1 along with the concerned parameters, pillar length (PL) and minimum interpillar distance (MIPD). For future discussion, we will designate and differentiate these systems in terms of "PL##_XXX_MIPD&&" terminology, where PL corresponds to pillar length; MIPD corresponds to minimum interpillar distance; and "##" and "&&" correspond to the values of approximate pillar length (PL) and minimum separation distance between pillars from edges of the nanotubes (MIPD), respectively in Å. XXX corresponds to either GPH or CNT which signify a particular direction. For example, PL12_GPH_MIPD9 will correspond to a pillar graphene system in which pillar length is about 12 Å; minimum interpillar distance is about 9 Å; and nonequilibrium thermal conductivity simulation is being studied along graphene (GPH) direction. We have

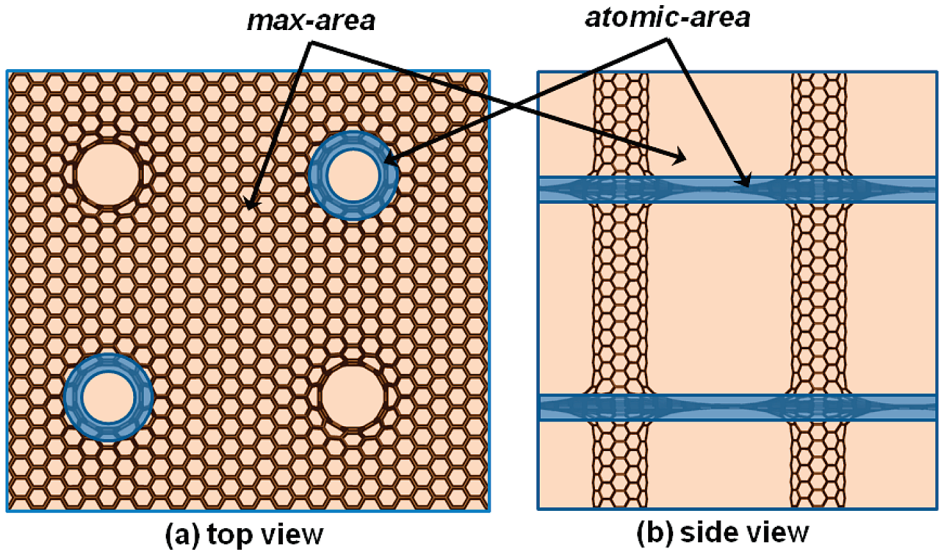

Figure 2. Schematic of different cross-sectional areas used for thermal conductivity calculations in pillared-graphene structures for heat flow along (a) nanotube-axis direction; (b) graphene-plane direction. The shaded region of max-area and atomic-area are also represented. The width of the shaded region in blue (atomic-area) was assumed to be 3.4 Å.

also performed nonequilibrium MD simulations on pure graphite and (6, 6) carbon nanotube structures in order to compare the thermal transport results of pillared-graphene structures with these pure allotropic forms. For current study, all systems were simulated using AIREBO force field[45] using molecular dynamics simulation package LAMMPS,[46] as provided by Sandia National Laboratories.

RESULTS AND DISCUSSION

We have categorized this section into three parts. First, a brief discussion regarding cross-sectional area employed for the thermal conductivity calculations is presented. Then, thermal conductivity results of various simulated pillared-graphene systems are discussed based on Fourier law formalism. Here, we describe the results of only one of the three studied systems (PL32_MIPD21) in detail as analysis strategy was same for all PG cases. (Here, XXX is dropped from terminology as both GPH and CNT simulations are discussed.) Finally, we compare and discuss the thermal conductivity values of pillared-graphene systems with pure graphite and (6,6) carbon nanotubes simulated systems and discuss the important governing parameters for thermal transport from a material design perspective.

Consideration of Cross-Sectional Area for Thermal Conductivity Calculations. In order to calculate, discuss, and compare thermal conductivity values of pillared-graphene structures, it is necessary to talk briefly about cross-sectional areas which are used in calculations due to significant spatial nonhomogeneity (empty space) in these structures (please refer to eq 1). One such cross-sectional area, perpendicular to heat flow, is the *overall* cross-sectional area of the pillared-graphene system that includes empty space. This area is most crucial from the perspective of material design. Another important area consists only of the region where the atoms are present, for example, the area of the annular shell in carbon nanotubes. Such an area has been repeatedly used in literature to calculate and predict thermal conductivity of carbon nanotubes, a similar spatially nonhomogeneous system at molecular length scale. As discussed later, this area turns out to be quite useful in the understanding of phonon scattering in the PG structures. For example, considering the latter area enables us to focus on the effect of phonon scattering at CNT−graphene junctions on in-plane thermal conductivity, avoiding nanotube length concerns on thermal conductivity which inherently appear if the former area is used.

To address these issues, we have considered two areas - maximum cross-sectional area, corresponding to overall system dimensions and atomic cross-sectional area, corresponding only to area where atoms are present - for the calculation for thermal conductivity values. We will refer to these areas as *max-area* and *atomic-area* in the remainder of the manuscript and discuss the relevance for their preferred usage in later sub-sections. These cross-sectional areas are schematically shown in Figure 2 for more clarity. Specifically, for atomic-area calculation in the CNT direction, (such as PL32_CNT_MIPD21), the cross-sectional area equivalent to *n* annular rings of width 3.4 Å was employed (*n* corresponds to the number of nanotube pillars at certain *z*-value). Similarly, for atomic-area calculation along graphene direction, we employed a cross-sectional area equivalent to *n* graphene sheets of width 3.4 Å. For the sake of completeness, both cross-sectional areas for simulated pillared-graphene systems are listed in Table 2.

Thermal Conductivity of Pillared-Graphene Systems. Figure 3 shows the cumulative heat flow as a function of time for PL32_MIPD21 systems for both studied directions.

TABLE 1. Specifications of Various Studied Systems

system studied	slab direction	replication/number of repeat units (no. of atoms)	final system sizes (*nm*) *X*, *Y*, *Z*
		Graphite (8 layers of graphene)	
G1	along *X*	32 repeat units (15360)	13.40, 3.63, 2.73
G2	along *X*	64 repeat units (30720)	26.80, 3.63, 2.73
G3	along *X*	128 repeat units (61440)	53.60, 3.63, 2.73
G4	along *X*	256 repeat units (122880)	107.20, 3.63, 2.73
		(6, 6) Carbon Nanotube	
CN1	along *Z*	25 repeat units (600)	3.0, 3.0, 6.07
CN2	along *Z*	50 repeat units (1200)	3.0, 3.0, 12.15
CN3	along Z	100 repeat units (2400)	3.0, 3.0, 24.30
CN4	along *Z*	200 repeat units (4800)	3.0, 3.0, 48.60
CN5	along *Z*	400 repeat units (9600)	3.0, 3.0, 97.19
CN6	along *Z*	800 repeat units (19200)	3.0, 3.0, 194.38
		Pillared-Graphene System (along Graphene Direction)	
PL12_GPH_MIPD9	along *X*	(8,2,2) unit cells (33280)	26.54, 6.70, 4.79
PL32_GPH_MIPD21	along *X*	(10,1,1) unit cells (33760)	58.43, 5.30, 6.48
PL12_GPH_MIPD21	along *X*	(10,1,1) unit cells (26080)	58.44, 5.30, 2.60
		Pillared- Graphene Systems (along Nanotube Directions)	
PL12_CNT_MIPD9	along *Z*	(2,2,8) unit cells (33280)	6.63, 6.70, 19.19
PL32_CNT_MIPD21	along *Z*	(1,1,10) unit cells (33760)	5.84, 5.30, 64.99
PL12_CNT_MIPD21	along *Z*	(1,1,10) unit cells (26080)	5.84, 5.30, 26.07

TABLE 2. Thermal Conductivity Results of Pillared-Graphene Systems

system studied	heat flow (eV/ps)	temperature gradient (K/nm)	atomic (max) cross-sectional area (nm^2)	thermal conductivity (W/m-K)
		Pillared-Graphene Systems (Along Graphene Direction)		
PL12_GPH_MIPD9	1.95	1.013	9.11 (32.09)	33.792 (9.60)[a]
PL32_GPH_MIPD21	0.96	0.492	3.60 (34.34)	86.608 (9.10)
PL12_GPH_MIPD21	1.06	0.548	3.60 (13.78)	86.242 (22.7)
		Pillared-Graphene Systems (Along Nanotube Direction)		
PL12_CNT_MIPD9	1.02	1.630	6.93 (43.79)	14.438 (2.25)
PL32_CNT_MIPD21	0.20	0.540	1.73 (30.97)	33.263 (1.86)
PL12_CNT_MIPD21	0.24	1.227	1.73 (30.97)	15.773 (0.88)

[a]Nonbracketed thermal conductivity values (atomic-area); bracketed thermal conductivity values (max-area).

It is clear from the figure that the overall heat flow along the graphene direction is higher than that along the nanotube direction. The figure also suggests the steady state was reached quickly, as the slopes of heat flow plots become similar with each other for hot (*black*) and cold (*red*) thermostated regions. Indeed, the two observations discussed above were true for all studied PG systems. This can be seen from the values of heat flow (in eV/ps) as listed in Table 2.

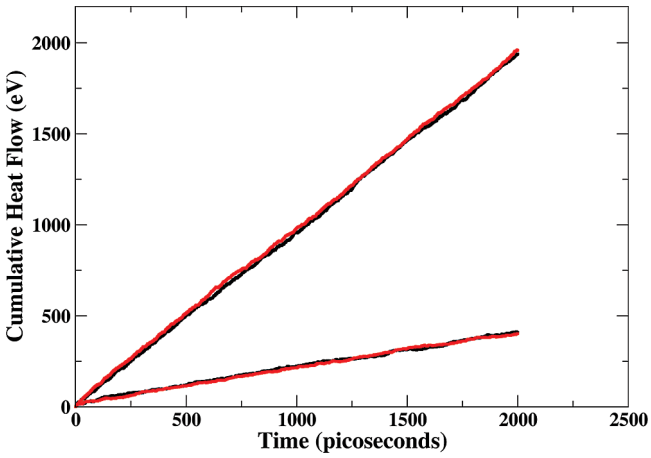

Figure 3. Cumulative heat flow along the direction of simulated slab as a function of time for pillared-graphene system (PL32_MIPD21). (Top plot) PL32_GPH_MIPD21; (bottom plot) PL32_CNT_MIPD21. Color scheme: (black) heat in the hot thermostated region; (red) heat flow out from the cold thermostated region.

Figure 4 shows the plot of induced temperature profile along the slab for PL32_MIPD21 systems along both directions. To avoid any bias in the time averaging of temperature across bins, the averaging was done only after temperature gradient profile got stabilized with respect to time (after 500 ps). The temperature gradient was calculated by fitting the middle section of the graphs (~25 nm) and is listed in Table 2. In addition, Figure 4 shows that the temperature profile is nonlinear in the vicinity of boundary layers. This is attributed to scattering of phonons at the boundary in temperature-controlled layers and is often observed in NEMD simulations of highly thermally conductive systems.[47]

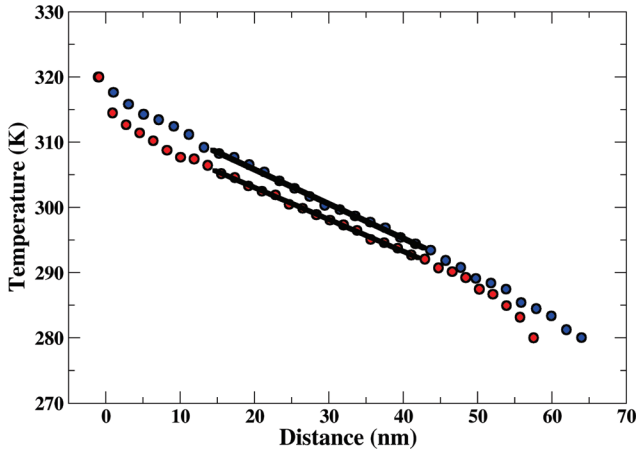

Figure 4. Temperature profile of pillared-graphene system (PL32_MIPD21) in the steady state as a function of slab length. Color scheme: (red) PL32_GPH_MIPD21; (blue) PL32_CNT_MIPD21. Black solid lines are least-squares fit to temperature profile data at the center of the unthermostated zone.

The thermal conductivity results of all three PG systems along nanotube and graphene sheet directions, are also listed in Table 2 for both cross-sectional areas. For all studied cases, we observed that the thermal conductivity along the graphene direction is significantly higher than along the nanotube direction. The results also suggested that interpillar distance and pillar length play a crucial role in determining overall thermal transport in these systems. The preliminary analysis of simulated PG systems led to several important concerns. (i) How does thermal conductivity of PG systems *scale* with that of pure allotropic systems under the similar system sizes? (ii) Does overall thermal conductivity of the PG systems *vary* with system size? (iii) What is the *specific role* of both components (CNT-pillar length as well as their interlayer distance) in dictating overall thermal transport in both perpendicular directions?

Comparison with Pure Systems. In order to address these concerns, we carried out thermal conductivity simulations of pure (6, 6) carbon nanotubes and planar graphite sheets for different system sizes based on similar simulation protocol as described for PG systems. The details of pure systems are listed in Table 1. For graphite simulations, 8-graphene sheets were stacked together in an AB type of layer stacking[14] to create the graphite model structure. The thermal conductivity of graphite is plotted in Figure 5 as a function of system size. The figure shows that thermal conductivity, λ, increases with system size and appears to saturate as the system size increases. Such power law behavior is often observed in highly thermally conductive systems in which characteristic mean-free-path is larger than the system size.[15,48,49] The figure also shows calculated values of λ for various studied PG systems along the graphene direction (GPH systems), based on atomic-area predictions. By using atomic-area, thermal conductivity in the graphene plane becomes independent of nanotube−pillar length. It allows us to understand the thermal transport limiting mechanisms, such as effects of CNT-graphene junctions on phonon scattering, within the plane. On the contrary, usage of *max-area* adds further complexity in the calculation of in-plane thermal conductivity of graphene, arising from the changes in cross-sectional area normal to heat flow due to consideration of pillar length. The plotted values in Figure 5 suggest that incorporation of CNT pillars in graphite sheets do provide scattering points at the junction, significantly reducing the thermal conductivity with respect to pure systems. The data also suggest that although the values of λ are relatively low, it is increasing with overall system size.

To understand that if it is truly the system size or is it the interpillar distance which governs the overall in-plane thermal conductivity, we performed one more NEMD simulation on another system, which we call 3X_PL12_GPH_MIPD9. 3X in front of "***3X***_PL12_GPH_MIPD9" corresponds to a system which is 3 times larger along X direction and has same pillar length and inter-pillar distances as of PL12_GPH_MIPD9. It can be thought as just simple replication of PL12_GPH_MIPD9 structure three times along *X* direction (graphene-plane direction). The thermal conductivity of this new system is also plotted in Figure 5 (orange). From the figure, it is clear that although the system size of 3X_PL12_GPH_MIPD9 is largest among all studied systems, λ does not follow the same trend. In fact, its conductivity value is very close to PL12_GPH_MIPD9 (3X_PL12_GPH_MIPD9 and PL12_GPH_MIPD9 have the same interpillar distance). This suggests that it is, indeed, the interpillar distance which governs the in-plane thermal conductivity of the

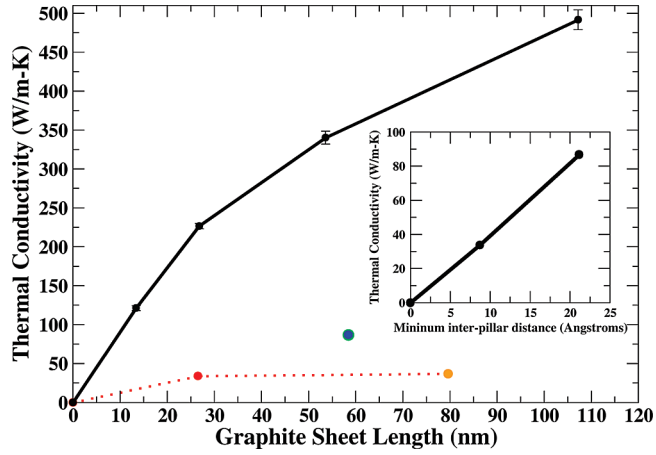

Figure 5. Thermal conductivity of graphite and pillared-graphene systems along the graphene plane direction based on atomic-area calculations: (black) pure graphite systems; (red) PL12_GPH_MIPD9; (green) PL32_GPH_MIPD21; (blue) PL12_GPH_MIPD21; (orange) 3X_PL12_GPH_MIPD9 (see text). The inset shows the thermal conductivity of PG systems along graphene direction as a function of minimum interpillar distance (MIPD). MIPD is the distance between the nearest pillars from the edges of the nanotubes (see Figure 1).

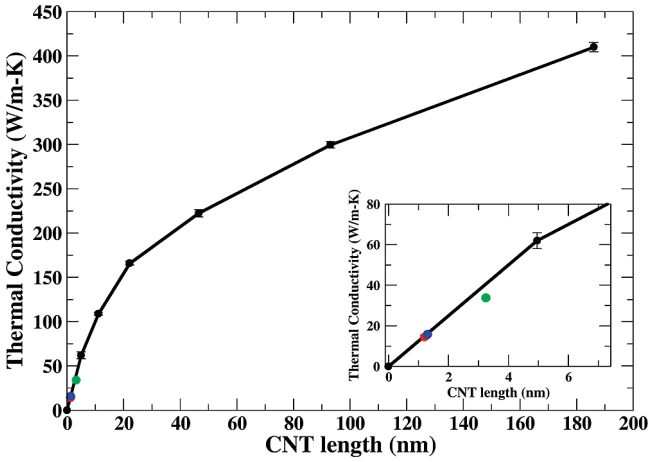

Figure 6. Thermal conductivity of (6, 6) carbon nanotubes and pillared-graphene systems along the nanotube direction based on atomic-area calculations: (black) pure carbon nanotube systems; (red) PL12_CNT_MIPD9; (green) PL32_CNT_MIPD21; (blue) PL12_CNT_MIPD21. The inset shows the data points of thermal conductivity values of PG systems along the CNT direction in better resolution along with CNT thermal conductivity (in black).

system rather than absolute system size along the heat flowing direction, which might have a little significance. This is more clearly seen in the inset of Figure 5, where thermal conductivity, λ, of the PG systems is plotted as a function of minimum interpillar distance (MIPD) instead of overall system size (refer to Figure 1 for MIPD). It is seen that λ increases linearly with MIPD at studied length scales. Such a phenomenon could be understood from the following reasoning. When the interlayer distance is large, the scattering of in-plane phonons will occur at longer distances (at the junctions). This, in turn, will increase the overall phonon mean-free-path leading to higher values of λ. With further increasing interpillar distances, λ in the graphite direction will approach that of a pure graphitic system. We would also like to mention that in all of our PGS studies, we do not expect any significant intersheet interaction for graphene, as the least simulated intersheet distance (pillar length) is 12 Å, at which van der Waals interactions become negligible. This is further confirmed from the results of PL12_GPH_MIPD21 and PL32_GPH_MIPD21 (same interpillar distance, different pillar length). Both systems have similar in-plane thermal conductivity as listed in Table 2, based on atomic-area considerations. The difference in such cases only arises because of geometric concerns when we consider *max-area* which incorporates nanotube pillar length in conductivity calculations (discussed later).

Along similar lines, results of thermal conductivity for (6,6) carbon nanotubes are plotted as a function of nanotube length in Figure 6. The conductivity values of nanotube also show size dependent behavior similar to graphite, and can be understood based on the similar arguments as discussed previously. Our predicted results are in good agreement with published literature.[24,50−53] Regarding length dependence of thermal conductivity, our results predict a power law with exponent ∼0.4 which lies well within predictable range in different studies for armchair (*n*,*n*) nanotubes.[24,52−54] The figure also shows calculated values of thermal conductivity for various studied PG systems along nanotube axial direction with respect to pillar length (instead of overall system size). As stated before, to compare the results with those of pure nanotube systems, we have used atomic-area based thermal conductivity values. It is quite remarkable that at studied length scales, calculated conductivity values of PG systems follow pure nanotube results very closely when plotted against nanotube pillar length. This trend can be seen more clearly in the inset of Figure 6. The longer the nanotube pillar length, the higher the conduction. Such behavior can again be attributed to the distance at which the scattering of phonons occurs along the nanotube direction (at CNT−graphene junction).

Considerations for Material Design. From the above discussion, phonon scattering at the junctions emerges as the crucial mechanism which limits thermal transport along graphene-plane and along nanotube axis. However, while designing these materials for thermal transport, additional geometric aspects should be analyzed, which also reveal the importance of overall cross-sectional area (max-area). In such a case, we note that both distances, pillar length and interpillar distance, affect overall thermal transport in either direction. For example, along the graphene direction, while minimum interpillar distance governs the phonon scattering and hence thermal conduction, the length of CNT pillars is also significant. Increasing pillar length will increase the effective cross-sectional area (max-area) for same number of graphene layers, reducing in-plane thermal conductivity. Similarly, interpillar distance also becomes a significant factor in determining effective thermal conductivity along nanotube direction. The more the number of pillars within certain cross-sectional area (lower value of interpillar distance), the higher the thermal transport along CNT-pillar direction. On the basis of above discussion, it is evident that both interpillar distance and pillar length, indeed, are crucial factors in governing overall in-plane and out-of-plane thermal transport.

SUMMARY AND CONCLUSIONS

In this article, we have investigated the thermal transport in a novel 3-D pillared-graphene architecture. At studied length scales, we find that pillar length and minimum interpillar distance are the two important parameters which govern thermal transport. On the basis of atomic-area thermal conductivity predictions, we conclude that phonon scattering at the CNT−pillar-graphene junctions is the governing mechanism which limit thermal transport in these systems. Owing to spatial in-homogeneity in these architectures, geometric

aspects also play a significant role toward thermal conductivity from material design perspective. We find that both minimum interpillar distance and pillar length are important parameters in deciding thermal conductivity in either direction. While one of the distances dictates phonon scattering length between CNT−graphene junctions, other distance determines overall cross-sectional area of the system. These points should be kept in mind while designing such template architectures for not only thermal transport but any flux related property. In regards to thermal conduction, we also postulate that since all atoms at the CNT−graphene junction are of the same atomic mass and same hybridization, such a junction will provide a significantly low resistance and allow the thermal energy to be transported in an efficient manner.

METHODS

Theory of Thermal Conductivity Calculation from NEMD Simulations. The Fourier law approach is based on the principle of heat conduction which states that under steady state conditions, the amount of heat flow per unit area in unit time is directly proportional to the temperature gradient at the cross-section.[55] This proportionality constant is widely known as thermal conductivity and is calculated as shown in eq 1.

$$\lambda = \frac{\frac{Q}{A\Delta t}}{\frac{dT}{dz}} \quad (1)$$

Here, Q is heat flow through the cross-sectional area A, Δt is the time for which heat is flowing and dT/dz is the steady state temperature gradient. A representative protocol for the calculation of $Q/A\Delta t$ and dT/dz from molecular dynamics simulations (which is used in this study) is briefly discussed below.

First of all, the system of interest is modeled as a thin slab with large aspect ratio along the heat flow direction and is equilibrated at desired temperature and pressure. Next, one boundary of the slab is heated to desired high temperature, T_{high}, and is kept at that temperature while the other boundary is cooled and kept at desired low temperature T_{low}. To keep the regions at their specified temperatures, energy is continuously added and taken off from the hot and cold regions during the course of the simulation, respectively. Energy addition or removal is done in terms of modifying kinetic energy by a velocity rescaling procedure in both hot and cold thermostat, respectively. In doing so, a temperature gradient is established across the slab. To calculate the temperature gradient, the slab is divided into a pre-defined number of thinner slabs with equal thickness. Thereafter, the temperature of each slab is calculated as follows.

$$T_i = \frac{1}{3N_i k_B} \sum_{k=1}^{N_i} m_k v_k^2 \quad (2)$$

where, N_i is number of atoms in i^{th} slab, m_k and v_k represent the mass and velocity of the atom k, respectively, and k_B is the Boltzmann constant. Furthermore, the calculated temperature for each slab T_i is averaged over the several picoseconds to get a smooth temperature profile. At last, the temperature gradient is calculated by the slope of resulting temperature profile.

Similarly, heat flux per unit area, $Q/(A\Delta t)$ is calculated as follows

$$\frac{Q}{A\Delta t} = \frac{1}{A\Delta t}\left\langle \frac{1}{2}\sum_{k=1}^{N_B} m_k(v_k^2 - vp_k^2) \right\rangle \quad (3)$$

where vp_k and v_k are the velocities of the atoms before and after rescaling to temperature of the thermostat, respectively. N_B is the number of atoms in the boundary layers. Once the temperature gradient and heat flux are known, the thermal conductivity is calculated using eq 1.

Simulations Protocol. The design of the pillared-graphene systems has been discussed in detail by Froudakis *et al.*[20] In brief, to create a nanotube−graphene junction for PG systems, (6, 6) carbon nanotubes of varying lengths were brought vertically within atomic distance close to a graphene sheet with a hole, whose diameter was similar to those of (6,6) nanotubes. This was followed by bond formation between end-atoms of nanotubes and graphene sheet using quantum calculations (DFT-BLYP/SVP level of theory) and subsequent relaxation of the system. The junction topology followed Euler's rule for polygons at the surface of closed polyhedron,[56] regarding creation of heptagons at the junction. These structures were later used for MD studies as discussed next.

Initially, the unit cells of all pillared-graphene structures (as shown in Figure 1) along with graphite and nanotube systems were minimized using a conjugate gradient algorithm. Thereafter, in order to achieve equilibrated structures at 300 K, all systems were subjected to following series of simulations: (A)constant volume (NVT) simulations for 100 ps, and (B) constant pressure (NPT) simulations for 300 ps (independent barostats in *X*-, *Y*-, and *Z*- directions).

At this stage, periodic boundary conditions were used in all directions. For all studied simulations and ensembles, a time step of 0.8 fs was used. After equilibration, the systems were replicated several times in either *X*-direction (along graphene-plane direction) or *Z*-direction (along nanotube-axis direction) to create the slab morphology. Thereafter, the system was further equilibrated using NPT simulations with independent directional barostats for 200 ps, followed by NVE simulations for 200 ps. The replication details along with final dimensions of all studied systems prior to NEMD simulations are listed in Table 1.

For nonequilibrium simulations, each studied elongated system was divided into 32 thin slabs of equal thickness (for longer pure (6,6) nanotube and graphite cases, we divided the elongated system in 64 thin slabs of equal thickness). Subsequently, one slab at the boundary was chosen and treated as the hot region while another slab on the other boundary was treated as the cold region. The system was set to be periodic in the other two directions perpendicular to heat flow. For current study, the hot region was kept at 320 K while the cold region was kept at 280 K. Then, NEMD simulations in microcanonical ensemble (NVE) were run for 2 ns in order to achieve the steady-state for heat flow, and data collected for subsequent analysis.

Acknowledgment. The authors are thankful for US Air Force Office of Scientific Research for the financial support. The authors also acknowledge T. Fisher for his helpful discussion during the course of this study.

REFERENCES AND NOTES

1. Sergent J. E.; Krum, A. *Thermal Management Handbook: For Electronic Assemblies*; McGraw-Hill Professional: New York, 1998.
2. Garimella, S. V. Advances in Mesoscale Thermal Management Technologies for Microelectronics. *Microelectron. J.* **2006**, *37*, 1165–1185.
3. Sazonova, V.; Yaish, Y.; Ustunel, H.; Roundy, D.; Arias, T. A.; McEuen, P. L. Tunable Carbon Nanotube Electromechanical Oscillator. *Nature* **2004**, *431*, 284–287.
4. Cao, Q.; Kim, H. S.; Pimparkar, N.; Kulkarni, J. P.; Wang, C.; Shim, M.; Roy, K.; Alam, M. A.; Rogers, J. A. Medium-Scale Carbon Nanotube Thin-Film Integrated Circuits on Flexible Plastic Substrates. *Nature* **2008**, *454*, 495–500.

5. Segal, D.; Nitzan, A.; Hänggi, P. Thermal Conductance through Molecular Wires. *J. Chem. Phys.* **2003**, *119*, 6840–6855.
6. Chang, C. W.; Okawa, D.; Majumdar, A.; Zettl, A. Solid State Thermal Rectifier. *Science* **2006**, *314*, 1121–1124.
7. Chang, C. W.; Okawa, D.; Garcia, H.; Majumdar, A.; Zettl, A. Nanotube Phonon Waveguide. *Phys. Rev. Lett.* **2007**, *99*, 045901.
8. Tyler, W. W.; Wilson, A. C., Jr. Thermal Conductivity, Electrical Resistivity, and Thermoelectric Power of Graphite. *Phys. Rev.* **1953**, *89*, 870–875.
9. Wei, L.; Kuo, P. K.; Thomas, R. L.; Banholzer, W. F.; Anthony, T. R. Thermal Conductivity of Isotopically Modified Single Crystal Diamond. *Phys. Rev. Lett.* **1993**, *70*, 3764–3767.
10. Hone, J.; Whitney, M.; Zettl, A. Thermal Conductivity of Single-Walled Carbon Nanotubes. *Synth. Met.* **1999**, *103*, 2498–2499.
11. Kim, P.; Shi, L.; Majumdar, A.; McEuen, P. L. Thermal Conductivity of Single-Walled Carbon Nanotubes. *Phys. Rev. Lett.* **2001**, *87*, 215502.
12. Balandin, A. A.; Ghosh, S.; Bao, W.; Calizo, I.; Teweldebrhan, D.; Miao, F.; Lau, C. N. Superior Thermal Conductivity of Single-Layer Graphene. *Nano Lett.* **2008**, *8*, 902–907.
13. Berber, S.; Kwon, Y.-K.; Tománek, D. Unusually High Thermal Conductivity of Carbon Nanotubes. *Phys. Rev. Lett.* **2000**, *84*, 4613–4616.
14. Kelly B. T. *Physics of Graphite*; Applied Science Publishers: London, 1981.
15. Che, J.; Cagin, T.; Goddard, W. A., III. Thermal Conductivity of Carbon Nanotubes. *Nanotechnology* **2000**, *11*, 65–69.
16. Biercuk, M. J.; Llaguna, M. C.; Radosavljevic, M.; Hyun, J. K.; Johnson, A. T.; Fischer, J. E. Carbon Nanotube Composites for Thermal Management. *Appl. Phys. Lett.* **2002**, *80*, 2767–2769.
17. Chalopin, Y.; Volz, S.; Mingo, N. Upper Bound to the Thermal Conductivity of Carbon Nanotube Pellets. *J. Appl. Phys.* **2009**, *105*, 084301.
18. Stankovich, S.; Dikin, D. A.; Dommett, G. H. B.; Kohlhaas, K. M.; Zimney, E. J.; Stach, E. A.; Piner, R. D.; Nguyen, S. T.; Ruoff, R. S. Graphene-Based Composite Materials. *Nature* **2006**, *442*, 282–286.
19. Ramanathan, T.; Abdala, A. A.; Stankovich, S.; Dikin, D. A.; Herrera-Alonso, M.; Piner, R. D.; Adamson, D. H.; Schniepp, H. C.; Chen, X.; Ruoff, R. S.; *et al.* Functionalized Graphene Sheets for Polymer Nanocomposites. *Nat. Nanotechnol.* **2008**, *3*, 327–331.
20. Dimitrakasis, G. K.; Tylianakis, E.; Froudakis, G. E. Pillared Graphene: A New 3-D Network Nanostructure for Enhanced Hydrogen Storage. *Nano Lett.* **2008**, *8*, 3166–3170.
21. Li, Y.-F.; Li, B.-R.; Zhang, H.-L. The Computational Design of Junctions from Carbon Nanotubes and Graphene Nanoribbons. *Nanotechnology* **2009**, *20*, 225202.
22. Wu, X.; Zeng, X. C. Periodic Graphene Nanobuds. *Nano Lett.* **2009**, *9*, 250–256.
23. Wu, G.; Li, B. Thermal Rectification in Carbon Nanotube Intramolecular Junction: Molecular Dynamics Calculations. *Phys. Rev. B* **2007**, *76*, 085424.
24. Yang, N.; Zhang, G.; Li, B. Thermal Rectification in Asymmetric Graphene Ribbons. *Appl. Phys. Lett.* **2009**, *95*, 033107.
25. Noya, E. G.; Srivastava, D.; Menon, M. Heat-Pulse Rectification in Carbon Nanotube Y Junctions. *Phys. Rev. B* **2009**, *79*, 115432.
26. Alaghemandi, M.; Algaer, E.; Böhm, M. C.; Müller-Plathe, F. The Thermal Conductivity and Thermal Rectification of Carbon Nanotubes Studied Using Reverse Non-equilibrium Molecular Dynamics Simulations. *Nanotechnology* **2009**, *20*, 115704.
27. Wei, D.; Liu, Y. Intramolecular Junctions of Carbon Nanotubes. *Adv. Mater.* **2008**, *20*, 2815–2841.
28. Osman, M. A.; Srivastava, D. Temperature Dependence of the Thermal Conductivity of Single-Wall Carbon Nanotubes. *Nanotechnology* **2001**, *12*, 21–24.
29. Yao, Z.; Wang, J.-S.; Li, B.; Liu, G.-R. Thermal Conduction of Carbon Nanotubes Using Molecular Dynamics. *Phys. Rev. B* **2005**, *71*, 085417.
30. Bi, K.; Chen, Y.; Yeng, J.; Wang, Y.; Chen, M. Molecular Dynamics Simulation of Thermal Conductivity of Single-Wall Carbon Nanotubes. *Phys. Lett. A* **2006**, *350*, 150–153.
31. Che, J.; Cagin, T.; Deng, W.; Goddard III, W. A. Thermal Conductivity of Diamond and Related Materials from Molecular Dynamics Simulations. *J. Chem. Phys.* **2000**, *113*, 6888–6900.
32. Angadi, M. A.; Watanabe, T.; Bodapati, A. Thermal Transport and Grain Boundary Conductance in Ultrananocrystalline Diamond Thin Films. *J. App. Phys.* **2006**, *99*, 114301.
33. Kawamura, T.; Kangawa, Y.; Kakimoto, K. Investigation of Thermal Conductivity of Nitride Mixed Crystals and Superlattices by Molecular Dynamics. *Phys. Stat. Sol., C* **2006**, *3*, 1695–1699.
34. Feng, X.-L.; Li, Z.-X.; Guo, Z.-Y. Molecular Dynamics Simulation of Thermal Conductivity of Nanoscale Thin Silicon Films. *Microscale Thermophys. Eng.* **2003**, *7*, 153–161.
35. Phillpot, S. R.; Schelling, P. K.; Keblinski, P. Interfacial Thermal Conductivity: Insights from Atomic Level Simulation. *J. Mater. Sci.* **2005**, *40*, 3143–3148.
36. Yoon, Y.; Car, R.; Srolovitz, D. J.; Scandolo, S. Thermal Conductivity of Crystalline Quartz from Classical Simulations. *Phys. Rev. B* **2004**, *70*, 012302.
37. Chantrenne, P.; Raynaud, M.; Baillis, D.; Barrat, J. L. Study of Phonon Heat Transfer in Metallic Solids from Molecular Dynamic Simulations. *Microscale Thermophys. Eng.* **2003**, *7*, 117–136.
38. Chiritescu, C.; Cahill, D. G.; Nguyen, N.; Johnson, D.; Bodapati, A.; Keblinski, P.; Zschack, Z. Ultralow Thermal Conductivity in Disordered, Layered WSe_2 Crystals. *Science* **2007**, *315*, 351–353.
39. Varshney V.; Patnaik S. S.; Muratore, C.; Roy, A. K.; Voevodin, A. A.; Farmer, B. L. MD Simulations of Molybdenum Disulphide (MoS_2): Force-Field Parameterization and Thermal Transport Behavior. *Comput. Mater. Sci.* 2010, doi:10.1016/j.commatsci.2009.12.009.
40. Yang, C. B.; Quan-Wen, H. Thermal Conductivity of Carbon Nanotubes Embedded in Solids. *Chin. Phys. Lett.* **2008**, *25*, 1392–1395.
41. Varshney, V.; Patnaik, S. S.; Roy, A. K.; Farmer, B. L. Heat Transport in Epoxy Networks: A Molecular Dynamics Study. *Polymer* **2009**, *50*, 3378–3385.
42. Liu, Q.-X.; Jiang, P.-X.; Xiang, H. Molecular Dynamics Study of the Thermal Conductivity of Nanoscale Argon Films. *Mol. Simul.* **2006**, *32*, 645–649.
43. Kubo, R.; Toda, M.; Hashitsume N.; Saito, N. *Statistical Physics II*; Springer: Berlin, 1985.
44. McGaughey, A. J. H.; Kaviany, M. Phonon Transport in Molecular Dynamics Simulations: Formulation and Thermal Conductivity Prediction. *Adv. Heat Trans.* **2006**, *39*, 169–256.
45. Brenner, D. W.; Shenderova, O. A.; Harrison, J. A.; Stuart, S. J.; Ni, B.; Sinnott, S. B. A Second-Generation Reactive Empirical Bond Order (REBO) Potential Energy Expression for Hydrocarbons. *J. Phys.: Condens. Matter* **2002**, *14*, 783–802.
46. Plimpton, S. J. Fast Parallel Algorithms for Short-Range Molecular Dynamics. *J. Comp. Phys.* **1995**, *117*, 1–19.
47. Schelling, P. K.; Phillpot, S. R.; Keblinski, P. Comparison of Atomic-Level Simulation Methods for Computing Thermal Conductivity. *Phys. Rev. B* **2002**, *65*, 144306.
48. Maruyama, S. A Molecular Dynamics Simulation of Heat Conduction in Finite Length SWNTs. *Phys. B* **2002**, *323*, 193–195.
49. Broido, D. A.; Mingo, N. Length Dependence of Carbon Nanotube Thermal Conductivity and the "Problem of Long Waves". *Nano Lett.* **2005**, *5*, 1221–1225.

50. Gu, Y.; Chen, Y. Thermal Conductivities of Single-Walled Carbon Nanotubes Calculated from the Complete Phonon Dispersion Relations. *Phys. Rev. B* **2006**, *76*, 134110.
51. Yamamoto, T.; Watanabe, K.; Hernandez, E. R. Mechanical Properties, Thermal Stability and Heat Transport in Carbon Nanotubes. *Top. Appl. Phys.* **2008**, *111*, 165–194.
52. Rui-Qin, P.; Zi-Jian, X.; Zhi-Yuan, Z. Length Dependence of Thermal Conductivity of Single-Walled Carbon Nanotubes. *Chin. Phys. Lett.* **2007**, *24*, 1321–1323.
53. Shiomi, J.; Maruyama, S. Molecular Dynamics of Diffusive-Ballistic Heat Conduction in Single-Walled Carbon Nanotubes. *Jpn. J. Appl. Phys.* **2008**, *47*, 2005–2009.
54. Stoltz, G.; Lazzeri, M.; Mauri, F. Thermal transport in isotopically disordered carbon nanotubes: A comparison between Green's functions and Boltzmann approaches. *J. Phys.: Condens. Matter* **2009**, *21*, 245302.
55. Anderson, C. V. D. R.; Tamma, K. K. An Overview of Advances in Heat Conduction Models and Approaches for Prediction of Thermal Conductivity in Thin Dielectric Films. *Int. J. Numer. Methods Heat Fluid Flow* **2004**, *14*, 12–65.
56. Crespi, V. H. Relations between Global and Local Topology in Multiple Nanotube Junctions. *Phys. Rev. B* **1998**, *58*, 12671.